JOURNAL OF THERMOPHYSICS AND HEAT TRANSFER
Vol. 18, No. 2, April–June 2004

Multiple Scattering of Laser-Beam Radiation

H. F. Nelson*
University of Missouri–Rolla, Rolla, Missouri 65409-0050

This paper summarizes the experiential radiation-scattering research done at the University of Missouri–Rolla over the past 25 years. Complimentary theoretical studies are used to interpret the results. Anisotropic, multiple scattering is studied. The scattering situation is two-dimensional and cylindrical because the laser beam is incident normal to the upper surface of the scattering medium. Backscattered radiation in the normal direction is predicted and measured as a function of the distance from the incident laser beam. The influence of anisotropic scattering can be reduced to an effective isotropic scattering through the use of the asymmetry factor. Transmitted radiation is predicted and measured as a function of the distance from the incident laser beam. Effects of the angular details of the scattering phase function tend to become washed out at large optical depths. Side-scattered radiation in the radial direction is predicted and measured as a function of the distance below the upper surface of the scattering medium. Side-scattering measurements for optically thin media compare well with single scattering theory. Effects of multiple scattering on polarization are discussed. Polarization tends to make two-dimensional problems three-dimensional and requires the solution of the vector radiation transport equation.

Nomenclature

C_{sca} = scattering cross section, cm^2
c = scattering cross section divided by scattering particle volume, 1/cm
d = scattering particle diameter, μm
G = function $G(\tau_r; \omega, \tau_0)$, see Eq. (7)
g = asymmetry factor
I = radiation intensity, W/cm^2-strad
I_i = incident radiation intensity, W/cm^2-strad
$J_0(x)$ = zeroth-order Bessel function
L = depth of the scattering medium, cm
ℓ = transmission distance, cm
N = particle number density, particles/cm^3
n = relative real index of refraction of scattering particle to water
n_m = refractive index of liquid carrier medium = 1.33 for water at $\lambda_0 = 0.6328$ μm
$P(\Theta)$ = scattering phase function
P_i = incident power on the medium, $\pi r_0^2 I_i$, W
P_{90} = scattering phase function at $\Theta = 90$ deg
R = radius of the scattering medium, cm
R_0 = inside radius of detector barrel, 0.169 cm
r = radial distance from center of laser beam, cm
r_0 = effective radius of laser beam, cm
V = voltage reading of the detector, V
x = particle size parameter, $n_m \pi d/\lambda_0$
z = distance into media normal to the surface, cm
β = attenuation coefficient, $\sigma + \kappa$, 1/cm
$\delta(x)$ = Dirac delta function, where $a \le x_0 \le b$,

$$\int_a^b f(x)\delta(x - x_0)\,\mathrm{d}x = f(x_0)$$

η = particle volume concentration, $N\pi d^3/6$
Θ = angle between incident and scattered ray, deg
θ = polar angle for incident laser beam, deg
$\bar{\theta}$ = effective acceptance angle of detector, 2.10 deg
κ = absorption coefficient, 0.005 1/cm for water at $\lambda_0 = 0.6328$ μm
λ_0 = wavelength of the laser in air, 0.6328 μm
μ = arccos θ
ρ_N = normal reflectance, $(n_m - 1)^2/(n_m + 1)^2$
σ = scattering coefficient, $= \eta c$, $= NC_{\text{sca}}$, 1/cm
τ_0 = optical depth, $(\sigma + \kappa)L = \beta L$
τ_R = scattering media optical radius, $(\sigma + \kappa)R = \beta R$
τ_r = radial optical coordinate, $(\sigma + \kappa)r = \beta r$
τ_{r_0} = effective optical coordinate of incident (laser) beam, $(\sigma + \kappa)r_0 = \beta r_0$
ϕ = azimuthal angle for incident laser beam, deg
ω = single scattering albedo, $= \sigma/\beta$

Superscript

$*$ = effective value

Introduction

THIS paper reviews the integrated theoretical and experiential radiation-scattering research done at the University of Missouri–Rolla (UMR) over the past 25 years. The research program was motivated by a desire to obtain a better understanding of two-dimensional, multiple, anisotropic scattering. This paper is written in chronological fashion. Some of the initial published research results became outdated in later years, as a result of a vastly increased understanding of the theory and experiment.

The scattering medium geometry was two-dimensional and cylindrical because the laser beam was incident normal to the top of the scattering media. The theory and experiments were for a laser incident at the top center of a tank containing distilled water with white latex paint, or well-characterized latex spheres, suspended in the water to form the scattering medium. Polarization effects were not considered. Backscattered radiation and transmission were predicted and measured as a function of the radial distance from the incident laser beam. Radial-scattered radiation was measured and predicted as a function of depth of the scattering medium.

Scattering of electromagnetic radiation is important in many fields such as visibility, astrophysics, biology, remote sensing, and laser interaction with materials. Particular applications occur in astrophysics, biology, chemistry, laser interaction, metallurgy, meteorology, remote sensing, and visibility.

Multiple scattering becomes important as the number density of scattering centers or radiation path length increases. In many

Present as Paper 2003-3904 at the 36th Thermophysics Conference, Orlando, FL, 23 June 2003; received 30 June 2003; revision received 4 September 2003; accepted for publication 5 September 2003.

*Professor of Aerospace Engineering, Thermal Radiation Transfer Group, Department of Mechanical and Aerospace Engineering and Engineering Mechanics. Associate Fellow AIAA.

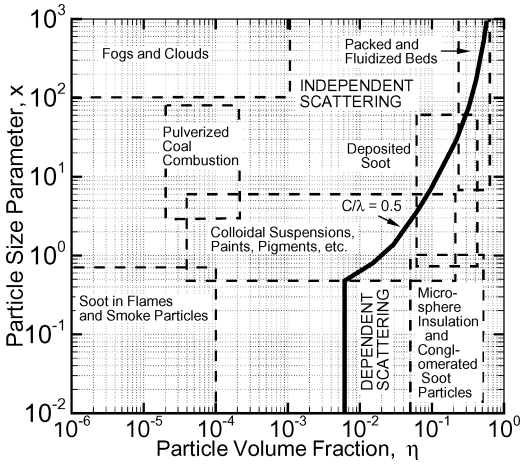

Fig. 1 Scattering regime map for independent and dependent scattering.[1]

situations the scattering is also multidimensional. Multidimensional scattering examples are dispersion of a source of illumination (searchlight problem), attenuation of radiation from a bolt of lightning by falling raindrops, and dispersion of laser radiation as it passes through a scattering medium. In each of these examples, the laser radiation is dispersed radially, as well as axially. The situations are complicated because the scattering is anisotropic.

Radiative properties of a cloud of spherical particles interacting with laser radiation of wavelength λ_0 are governed by three independent, nondimensional parameters: complex index of refraction $= n_m - i\kappa$; size parameter, $(x) = n_m \pi d/\lambda_0$; and clearance-to-wavelength ratio $= C/\lambda_0$, where C is the center-to center distance between particles. If the scattering is independent $(C/\lambda_0 \geq 1)$, only the first two parameters are needed. Figure 1 shows a scattering regime map for independent and dependent scattering.[1] It maps out the $x - \eta$ areas where various scattering problems are important. Dependent scattering effects can be ignored as long as $\eta \leq 0.006$. The range of parameters for the UMR research program was $6 \times 10^{-6} \leq \eta \leq 7 \times 10^{-4}$ and $0.20 \leq x \leq 6.7$. Thus, all of the research done at UMR and reviewed here is in the independent scattering regime. The research was generally in the range for problems like soot in flames, colloidal suspensions, and pulverized coal combustion.

Theory

Initially, the theory for the radial distribution of the backscattered radiation in the normal direction was developed for the following assumptions[2,3]: 1) steady-state; 2) independent scattering; 3) coherent scattering; 4) no polarization effects, scalar transport; 5) two-dimensional medium; 6) homogeneous media; 7) nonemitting media; 8) isotropic scattering; and 9) $n_m = 1$.

Incident Radiation

The laser beam was incident normal to the surface of the scattering medium. The radial variation of the laser beam was Gaussian, so that the incident intensity was given by

$$I^+(\tau_r, \mu, \phi) = I_i \delta(\mu - 1)\delta(\phi) \exp\left[-\left(\tau_r / \tau_{r_0}\right)^2\right] \tag{1}$$

where

$$\tau_{r_0} = (NC_{\text{sca}} + \kappa) r_0 = (\sigma + \kappa) r_0 = \beta r_0 \tag{2}$$

and

$$\tau_r = (NC_{\text{sca}} + \kappa) r = (\sigma + \kappa) r = \beta r \tag{3}$$

The resulting incident radiative flux is $I_i \exp(-\tau_r^2/\tau_{r_0}^2)$ W/cm^2, and the incident power is $\pi r_0^2 I_i$ W.

Scattering Phase Function

When the wavelength of the radiation is small compared to the particle diameter $(x \geq 1)$, diffraction around the particles gives rise to a sharp forward peak in the scattering phase function. Crosbie and Davidson[4] studied the use of Dirac delta function approximations to represent the angular variation of the single scattering phase function for large x. The phase function can be approximated as a spike in the forward direction $(\Theta = 0)$ plus an isotropic part

$$P(\Theta) = 2g\delta(1 - \cos\Theta) + (1 - g) \tag{4}$$

where g is defined as

$$g = \frac{1}{2} \int_0^{\pi} \cos\Theta P(\Theta) \sin\Theta \, \mathrm{d}\Theta \tag{5}$$

Note that $g = 0$, for isotropic scattering, $g = 1$ for pure forward scattering, and $g = -1$ for pure backward scattering. The parameter g is the fundamental phase function similarity parameter.[5]

Solution of Transport Equation

The theoretical analysis yields the normal backscattered intensity for large r/r_0 as

$$I\left(\tau_r^*\right) = I_i (r_0/r)^2 G\left(\tau_r^*; \omega^*, \tau_0^*\right) \tag{6}$$

where

$$G\left(\tau_r^*; \omega^*, \tau_0^*\right) = \frac{\omega^*}{8\pi} \int_0^{\infty} t J_0(t) R\left(\frac{t}{\tau_r^*}; \omega^*, \tau_0^*\right) \mathrm{d}t \tag{7}$$

and where the effective optical properties are

$$\tau_{r_0}^* = (1 - \omega g)\tau_{r_0}, \qquad \tau_r^* = (1 - \omega g)\tau_r \tag{8}$$

and

$$\tau_0^* = (1 - \omega g)\tau_0, \qquad \omega^* = \frac{\omega(1 - g)}{(1 - \omega g)} \tag{9}$$

in which

$$\tau_0 = (NC_{\text{sca}} + \kappa)L, \qquad \omega = \frac{NC_{\text{sca}}}{(NC_{\text{sca}} + \kappa)} \tag{10}$$

The quantity $G(\tau_r^*; \omega^*, \tau_0^*)$ is the intensity leaving normal to the medium when the medium is exposed to radially varying collimated radiation. Equation (6) has been numerically investigated for a wide range of parameters by Crosbie and Dougherty.[6–8] The effective optical properties are defined here because they will turn out to be important in correlating the theoretical and experimental results.

For a pure scattering $(\omega = 1)$, semi-infinite $(\tau_0^* \approx \infty)$ medium, $G(\tau_r^*; \omega^*, \tau_0^*)$ is a function only of τ_r^* (Ref. 7). The maximum value of $G(\tau_r^*, 1, \infty)$ is 0.04331 and occurs at $\tau_r^* = 3.345$ (Refs. 2 and 3).

Experiment

The experiential backscatter situation is shown schematically in Fig. 2. The experiment was designed to model a cylindrically symmetric, infinite/finite-depth scattering medium. The source was a He–Ne laser at $\lambda_0 = 0.6328$ μm. A glass tank was used to contain the scattering medium. The tank was fitted with a bottom, which was sprayed with highly absorbing black paint (diffusely reflecting with reflectance less than 2%). The side-wall effects were negligible.

The scattering medium was composed of well-characterized, spherical, latex particles immersed in distilled water.[†] The amount of scattering was controlled by the concentration of latex particles. The laser beam was incident normal to the upper surface of the scattering medium, so that the scattered radiation in the medium was a function of r and z.

[†]The first experiments (Ref. 2) used white latex paint for the scattering centers. The paint was very inexpensive, but the type of scattering particles and their size distribution were not accurately known.

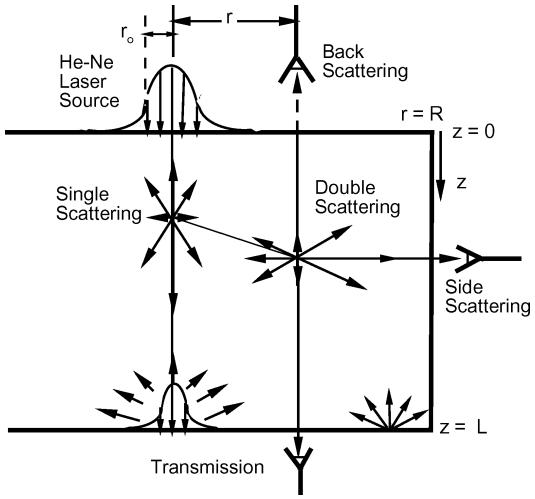

Fig. 2 Two-dimensional, semi-infinite/finite-depth, scattering situation. Receivers shown for backscattering, transmission, and side scattering. For transmission, $R = 15$ cm and $L = 45$ cm. For side scattering, $R = 5$ cm and $L = 10$ cm.

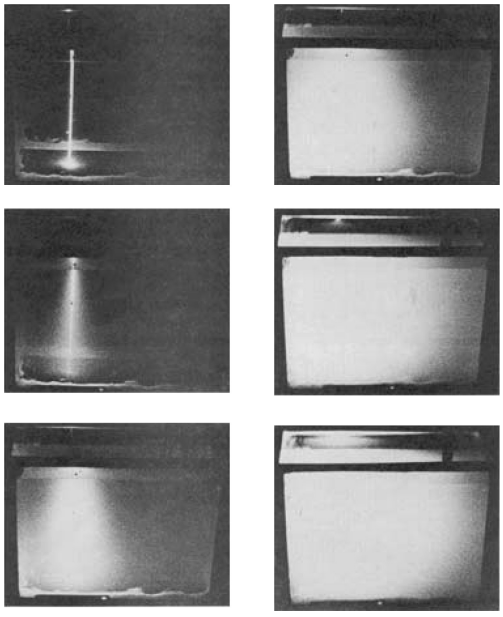

a) b)

Fig. 3 Composite of pictures of the scattering media for several concentrations of 1.011-μm-diam latex particles: a) top to bottom, $\eta = 6.23 \times 10^{-6}$, 3.79×10^{-5}, and 7.59×10^{-5}; b) top to bottom, $\eta = 1.58 \times 10^{-4}$, 3.79×10^{-4}, and 6.95×10^{-4} (Ref. 3).

Figure 3 is presented to show the dramatic effects of increasing the concentration of scattering particles (1.011 μm in diameter) on the scattered radiation. Note from the sequence of pictures that as η increases the apparent scattering volume of radiant energy expands. Though not presented in the figure, further addition of particles causes this scattering volume to collapse. This effect continues until only radiation reflected from the upper surface can be seen.

Data Reduction

The detector was designed to measure the normally backscattered radiation intensity as a function of radial distance from the laser beam as shown in Fig. 2. The ratio of reflected intensity to the incident laser-beam intensity is

$$\frac{I}{I_i} = \frac{1.53 \times 10^{-7}}{\pi}\left[\frac{r_0}{\bar{\theta} R_0}\right]^2 \frac{V}{P_i} \tag{11}$$

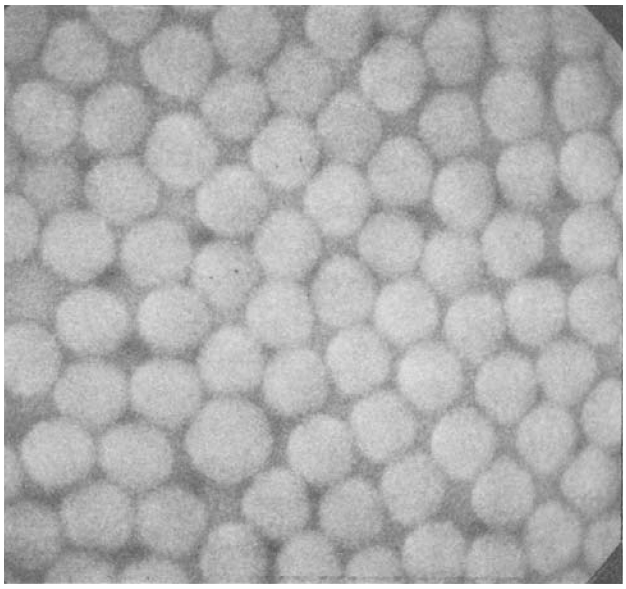

Fig. 4 Electron microscope picture of the $d = 1.011$-μm particles at a magnification of 10,000 (Ref. 3).

where $\bar{\theta} = 2.10$ deg $= 0.037$ rad, $R_0 = 0.169$ cm, and $r_0 = 0.20$ cm.[‡] The equation is very sensitive to the values of $\bar{\theta}$, R_0, and r_0. The sensitivity to r_0 can be eliminated by rearranging Eq. (11):

$$r^2 I \Big/ r_0^2 I_i = G\left(\tau_r^*; \omega^*, \tau_0^*\right) = 0.001273 r^2 (V/P_i) \tag{12}$$

The optical radius is written in terms of the particle volume concentration η from Eq. (3):

$$\tau_r = \left[\eta\left(6C_{\text{sca}}\Big/\pi d^3\right) + \kappa\right] r = (\eta c + \kappa) r = \beta r \tag{13}$$

The value of κ for distilled water is 0.005 1/cm at $\lambda_0 = 0.6328$ μm.

The value of C_{sca} for the scattering particles is known from Mie theory. C_{sca} was also measured by making transmission measurements through aqueous solutions containing known concentrations of scattering particles [$T = \exp - \beta\ell$] with a spectrophotometer.[9] The optical depth for the measurements was $\tau_\ell = (\eta c + \kappa)\ell = \beta\ell$. The value of c for latex particles is the scattering cross section divided by the particle volume, $6C_{\text{sca}}/\pi d^3$. The theoretical and experimental values of c were in excellent agreement.

The data were initially correlated using optical coordinates; however, later experience showed that the data correlated much better with the isotropic theory using effective optical coordinates. In other words, to compare the data to the simple theory [using Eq. (4) for the phase function], the actual experiential optical radius was multiplied by $(1 - \omega g)$ to yield the corresponding effective optical radius for the theoretical isotropic case τ_0^*. The $(1 - \omega g)$ factor approximately transforms the anisotropic problem to an effective isotropic problem.

Particle Characterization

The mean diameter of the polystyrene latex particles used for the scattering centers ranged from 0.03 to 1.011 μm. Standard deviations ranged from 0.0027 to 0.0125 μm for $d = 0.109$ to 1.011 μm. Figure 4 shows the uniformity of the $d = 1.011$ μm particles. The particles had approximately a neutral density in water (1.05 g/cc), and settling effects were not observed in a 24-hour period. Their refractive index was 1.593 (1.197 relative to water at $\lambda_0 = 0.6328$ μm), and they were assumed to be nonabsorbing ($\omega = 1$, $\kappa = 0$ for the particles). Table 1 lists the values of C_{sca}, x, and g for the latex particles used in the experiments. The parameters x and g are good indicators of the anisotropic character of small particles; however,

[‡]The values of $\bar{\theta}$, R_0, r_0, and P_i changed over the years for this research. The constant in Eq. (11) is gain dependent (see Refs. 2 and 3 for details).

Table 1 Latex particle parameters $\lambda_0 = 0.6328\ \mu$m and $n = 1.197$

d, μm	C_{sca}, μm^2	x	g
0.030	4.61×10^{-8}	0.198	0.00679
0.046	5.93×10^{-7}	0.304	0.0160
0.091	3.35×10^{-5}	0.601	0.0625
0.109	9.51×10^{-5}	0.720	0.0899
0.180	1.49×10^{-3}	1.19	0.253
0.312	0.0195	2.06	0.678
0.350	0.0335	2.31	0.718
0.481	0.131	3.18	0.809
0.500	0.154	3.30	0.822
0.527	0.192	3.48	0.835
0.801	0.963	5.29	0.898
1.011	2.150	6.68	0.917

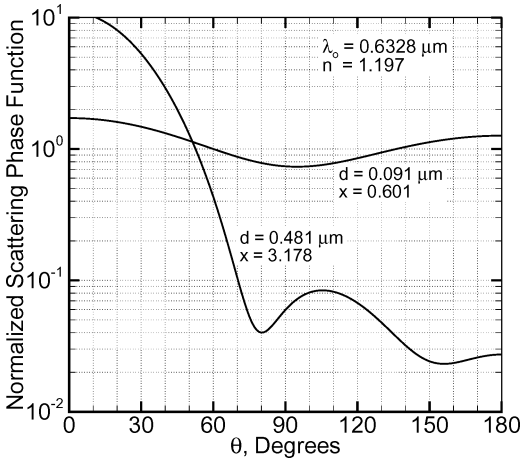

Fig. 5 Phase function for 0.109- and 0.481-μm-diam latex particles at $\lambda_0 = 0.6328\ \mu$m.

for large x ($x \gg 1$), g becomes oscillatory with x, and the relationship between x and g becomes quite complicated.[4] The anisotropic character of the 0.091- and 0.481-μm diam are shown in Fig. 5. The phase function for the 0.091-μm-diam particles is close to a Rayleigh distribution, whereas that of the 0.481-μm-diam particles is anisotropic with a large peak in the forward direction.

Backscattering

Initially, the theory and experiments were developed to approximate isotropic ($g = 0$), multiple scattering for $\tau_0 = \infty$, $\omega = 1$, and $n_m = 1$ as presented by Look et al.[2,3] The radial distribution of the backscattered radiation leaving a semi-infinite, cylindrical medium exposed to collimated laser radiation was predicted and measured using the geometry shown in Fig. 2. White latex paint was used in Ref. 2, and spherical latex particles were used in Ref. 3 to produce the scattering centers. All of the data in this research program were for $r/r_0 \gg 1$.

Figure 6 shows the theoretical solution for the backscattered radiation as a function of τ_r for two phase functions: isotropic and anisotropic (five-term case[10]) for $x = 2$.

The theoretical backscattered radiation leaving the media was expressed as a universal function of the optical radius $G(\tau_r, 1, \infty)$. Figure 7 shows $G(\tau_r; 1, \infty)[= r^2 I/(r_0^2 I_i)]$ for the measured anisotropic scattering.[3] The emerging intensity distribution curve shifts to larger τ_r as particle size increases. For a fixed particle concentration, changing τ_r represents changing radial distance from the laser beam. In general I decreases as τ_r increases for $r/r_0 \geq 1$. Multiplying I by r^2 gives the gives the curve shape shown in Fig. 7.

For very small concentrations of scattering centers, very little radiation will leave the medium outside the laser beam. The scattering is mainly single scattering. The theoretical solutions of Crosbie and

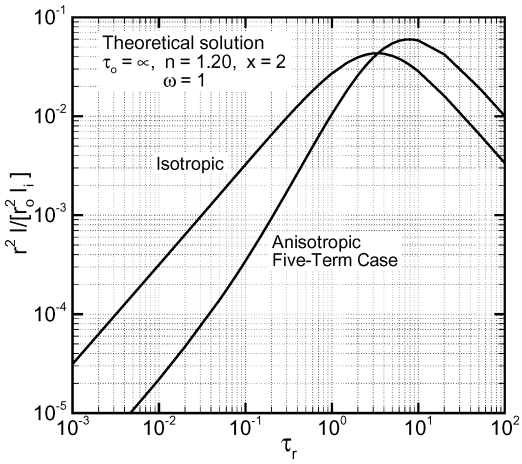

Fig. 6 Effect of phase function on the backscattered intensity as a function of τ_r (Ref. 10).

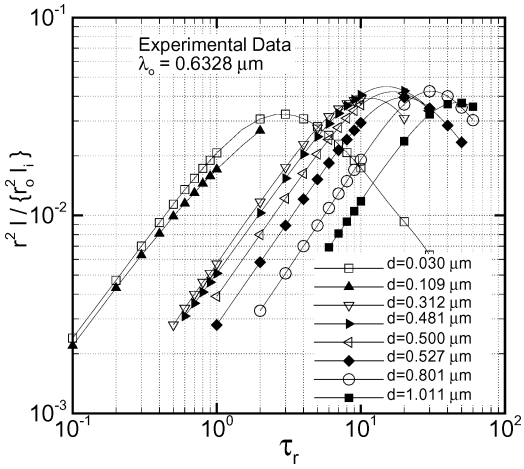

Fig. 7 Measured, nondimensional, backscattered intensity vs τ_r for various sized particles. $r_0 = 0.1$ cm (Ref. 3).

Dougherty[6] show that outside the beam the intensity I first falls off at a rate proportional to r_0/r. This behavior is double scattering. At larger values of r the backscattered intensity, I falls off at a rate proportional to $(r_0/r)^3$. This behavior is caused by higher-order scattering. The r^2 factor causes $r^2 I$ to increase with τ_r at small τ_r and to decrease with τ_r at large values of τ_r.[§]

Effect of g

Theoretically, anisotropic results can be reduced to a single effective isotropic curve, if one plots $G(\tau_r; 1, \infty)$ vs τ_r for $r/r_0 \geq 10$. Notice that all of the data on Fig. 7 did not collapse to a single curve. The theory shows that this condition can be remedied by use of the asymmetry factor g.[10] That is, the actual optical radius for the anisotropic case τ_r and the corresponding effective optical radius for the isotropic case τ_r^* are related by $(1 - g)$ as given by Eq. (18) when $\omega = 1$. The $(1 - g)$ factor transforms the anisotropic problem to an effective isotropic situation. When the data of Fig. 7 are adjusted using τ_r^*, it collapses into the plot shown in Fig. 8. The data appear to correlate better as τ_r^* increases. The 0.03-μm data do not correlate as well as the rest because the 0.03 particles were not as well characterized.

The reader is reminded of the physical situation of the preceding research, that is, the detector is a large distance from the incident beam ($r \gg r_0$, $\omega \approx 1$, $n_m = 1$, and $\tau_0 \approx \infty$. In addition g has a high dependency on x, as pointed out by Crosbie and Davidson.[4] The

[§]The factor $(r/r_0)^2$ will be used in the radiation intensity data presentation.

Table 2 Effective scattering parameters for latex particles in water at $\lambda_0 = 0.6328$ μm and $n = 1.197$

d, μm	x	g	c(theory), 1/cm	c(exp),[a] 1/cm
0.046[b]	0.30	0.016	115	115
0.180	1.19	0.253	4,850	5,211
0.350	2.31	0.718	14,850	15,085

[a]From transmission measurements.
[b]Experimental data used to characterize $d = 0.046$ particles.

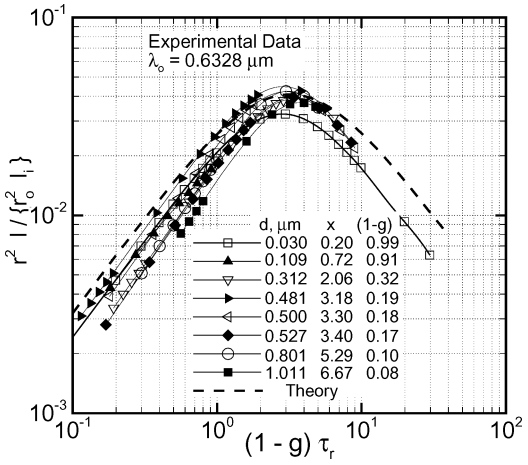

Fig. 8 Measured, nondimensional, backscattered intensity vs τ_r^* for various sized particles. Theory is isotropic for $\tau_0 = \infty$, $\omega = 1$, and $n_m = 1$ (Ref. 3).

values of x in the present experiments are in the region where g increases with x.

Effect of τ_0^*, n_m, and ω^*

The effects of τ_0, the optical depth of the media, were studied by Nelson et al.[11] The physical situation modeled finite L and is schematically shown in Fig. 2 so that the scattered radiation in the medium was a function of r and z. In this work the effect of the air–water interface n_m was accounted for, and the theoretical solution for the universal factor $G(\tau_r^*; \omega^*, \tau_0^*)$ was used. This improved the results of Refs. 2 and 3.

Experimentally measured values were used for c (Ref. 11). Theoretical values of x and g were obtained assuming a uniform size distribution for d (from the supplier) for the 0.18 and 0.35-μm particles and using $d = 0.0456$ μm for the smallest particles. The value of $d = 0.0456$ μm, and in turn x, g, and c (theory), for the small particles was obtained from the experimental value of c because the particle diameter for these particles was not well characterized. The values are given in Table 2. Measured and theoretical values of c in Table 2 show good agreement for all three diameters.

The assumption that $n_m = 1$ is inaccurate; however, it significantly reduced the numerical complexity of the theoretical analysis.[12] A single- and double-scattering analysis including the effects of refractive index shows that the backscattered intensity should be reduced by $(1 - \rho_N)^2/n_m^2$ (Refs. 13–16). This factor cannot be used over the entire optical radius range for pure scattering ($\omega = 1$), semi-infinite media ($\tau_0 = \infty$) because all of the incident energy must be backscattered. An analysis including multiple-scattering effects suggests shifting τ_r^* by $(1 - \rho_N)^2/n_m^2$. This approximation for pure-scattering, semi-infinite media is strictly valid only for τ_r in the thin region. The trends of this interface model are consistent with theory, even though it is a very simple model.

Figure 9 presents theoretical calculations that show the large effect of ω on the backscattered intensity as a function of τ_r. Note the large effect of small changes in ω at large $\tau_r \geq \approx 5$ (Ref. 10).

Figures 10–12 present $r^2 I/(r_0^2 I_i \omega^{*2})$ vs τ_r^*/n_m^2 for 0.046-, 0.18-, and 0.35-μm-diam scattering particles, respectively. The $1/\omega^{*2}$ in the ordinate and the τ_r^*/n_m^2 factor in the abscissa improve the agreement between theory and experiment at small τ_r^*. Note that $\rho_N \approx 0$ for the experiments. The $1/n_m^2$ shift seems to be reasonable because it improves agreement between the experimental data and the isotropic scattering theory. All of the optically thick experimental data fall off faster than the theory because of the sensitivity to absorption ω. Note that the curve shapes near the peak in Fig. 12 generally agree with the theory predictions of Fig. 9.

The data shown in Figs. 10 and 11 approach the asymptotic limit of $\tau_r^*/32$ at small τ_r^*/n_m^2 in agreement with the theory presented in

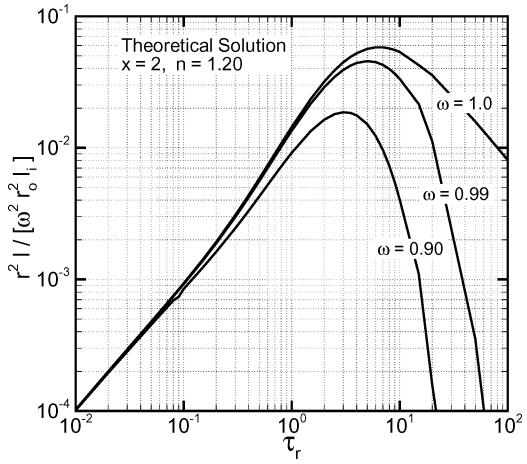

Fig. 9 Effect of absorption ω on anisotropic backscattered intensity vs τ_r for $\tau_0 = \infty$ (Ref. 10).

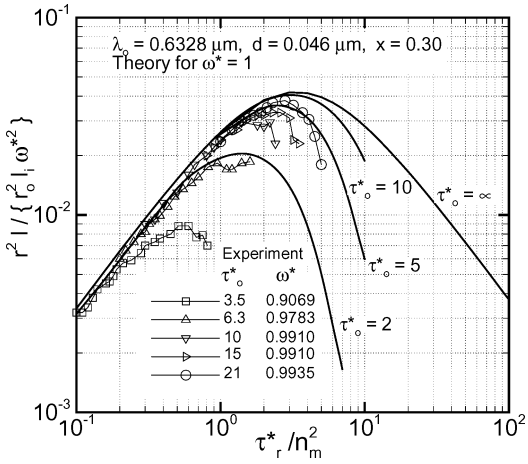

Fig. 10 Nondimensional backscattered intensity from the 0.046-μm-diam latex particles vs τ_r^*/n_m^2 (Ref. 11).

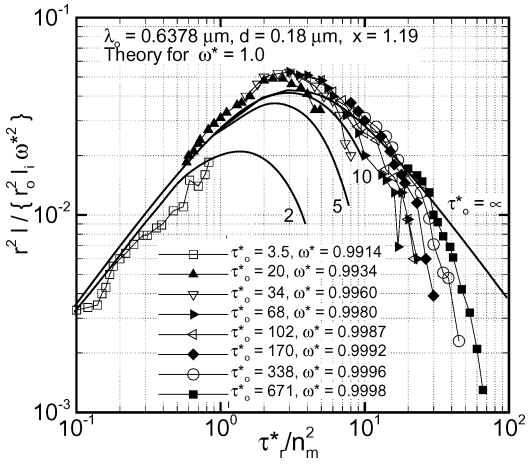

Fig. 11 Nondimensional backscattered intensity from 0.18-μm-diam latex particles vs τ_r^*/n_m^2 (Ref. 11).

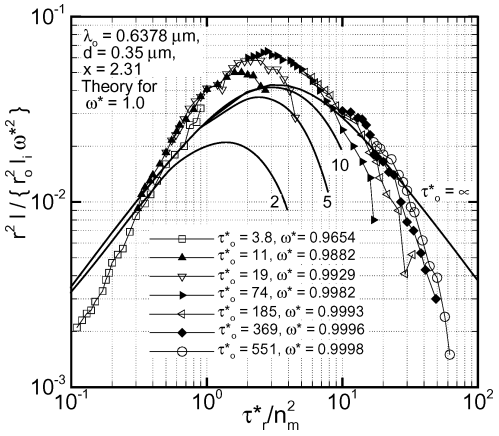

Fig. 12 Nondimensional backscattered intensity from 0.35-μm-diam latex particles vs τ_r^*/n_m^2 (Ref. 11).

Ref. 6. The data shown in Fig. 12 have a slightly different slope at small τ_r^*/n_m^2. This is generally in agreement with the theory of Crosbie and Lee,[12] who showed that the slope of the $r^2 I/(r_0^2 I_i \omega^{*2})$ vs τ_r^*/n_m^2 curve is a function of x. Their theoretical results showed that the slope is about the same for $x \leq \approx 1$ and then changes in an oscillating manner as x increases.

Preliminary data for backscattered radiation of a laser beam from a finite-depth medium were published by Look and Sundvold.[17,18] In these investigations, 0.261-μm-diam latex particles were used as the scattering centers. In Ref. 18, the particles were suspended in either distilled water ($n_m = 1.331$) or ethylene glycol ($n_m = 1.472$) to determine the influence of n_m. In Ref. 17, two laser wavelengths were used: 0.4414 and 0.6328 μm. The results indicated an influence because of n_m. At $\lambda_0 = 0.6328$ μm, an increase in n_m decreased the backscattered radiation, whereas, at $\lambda_0 = 0.4414$ μm, an increase in n_m increased the backscattered radiation.

In summary, the work of Ref. 11 extended the experiential τ_r^* results by a factor of 10 from the results in Refs. 2 and 3. In addition, it considered the influence of τ_0, ω, and n_m. These backscattered data are the only measurements in the literature for large τ_r^*. The results show that absorption in the medium and optical thickness of the medium are very important when $\tau_r^*/\tau_0^* \gg 1$.

Effect of Substrate

Comparisons of measurements and theory for backscattered radiation from scattering media ranging from optically thin to optically thick with either a reflecting or an absorbing substrate were presented by Nelson and Look.[19] The glass tank used in the experiments had $R = 26.6$ cm and a bottom that could be adjusted to change L from 26.6 to 3.325 cm. The intent of the research of Ref. 19 was to investigate the backscattering in the normal direction from finite optically thick media with black or white diffusely reflecting substrates in the presence of strong scattering.

Figures 13–16 present $r^2 I/(r_0^2 I_i \omega^{*2})$ vs τ_r^*/n_m^2 for $0.79 \leq \tau_0^* \leq 158$ for both white (reflectance greater than 98%) and black (reflectance less than 2%) substrates. The effective albedo is greater than 0.97 for all of the cases shown. Each figure contains three sets of data for the white substrate and three sets of data for the black substrate. The values of ω^* and τ_r^* are the same for each figure, whereas τ_0^* is different for each figure. The same scattering medium was used for each specific set of ω^* and $\tau_{r_0}^*$ values, and the depth was changed by raising the bottom to change the value of τ_0^*. Data are presented over the range from approximately $4\tau_{r_0}^* \leq \tau_r^* \leq 20\tau_{r_0}^*$. The solid lines in the figures represent the black substrate theoretical results for values of $\tau_0^* = \infty$, 10, 5, 2, 1, and 0.5 and $\omega^* = 1$ and $x = 2$.

Figure 13 shows the black and white substrate data for scattering media with $L/R = 2$. The values of τ_0^* are 6.46, 31.76, and 157.84. Reflecting or absorbing characteristics of the bottom do not influence the backscattered radiation in the normal direction, even for τ_0^* values as low as 6.5.

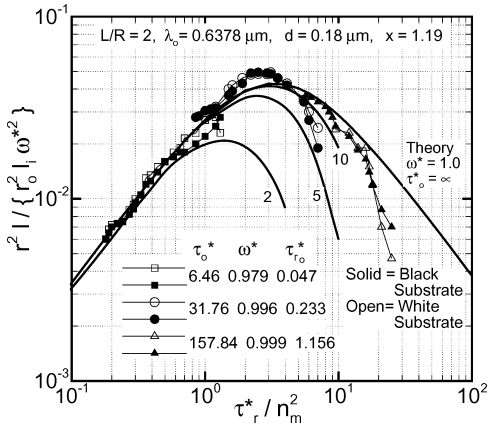

Fig. 13 Nondimensional backscattered intensity from 0.18-μm-diam polystyrene latex particles in distilled water vs contracted effective optical radius τ_r^*/n_m^2 ($L/R = 2$; ■, ▲, ●, black substrate; □, △, ○ white substrate).[19]

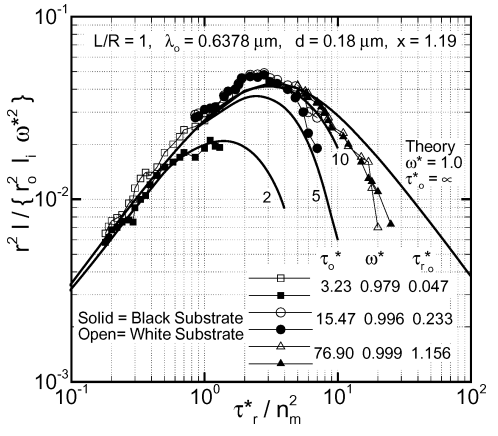

Fig. 14 Nondimensional backscattered intensity from 0.18-μm-diam polystyrene latex particles in distilled water vs contracted effective optical radius τ_r^*/n_m^2 ($L/R = 1$; ■, ▲, ●, black substrate; □, △, ○ white substrate).[19]

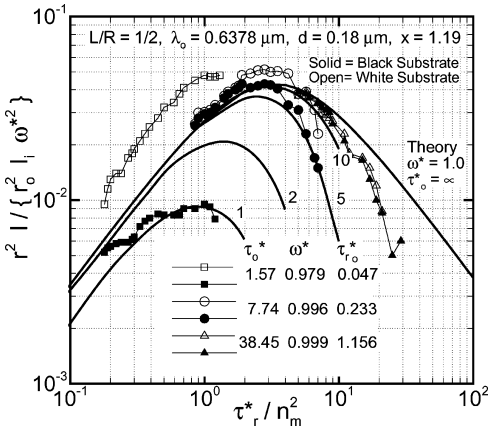

Fig. 15 Nondimensional backscattered intensity from 0.18-μm-diam polystyrene latex particles in distilled water vs contracted effective optical radius τ_r^*/n_m^2 ($L/R = 1/2$; ■, ▲, ●, black substrate; □, △, ○ white substrate).[19]

Figure 14 shows data for $\tau_0^* = 3.23$, 15.47, and 76.90 for $L/R = 1$. In this case, the backscattered radiation for τ_0^* greater than 15.5 is the same for both the black and white substrate. However, for $\tau_0^* = 3.2$ the backscattering from the medium with a white substrate is somewhat higher than that for the black substrate.

Figure 15 presents data for a scattering medium for $\tau_0^* = 1.57$, 7.74, and 38.45 ($L/R = 1/2$). The results are independent of the substrate when $\tau_0^* \geq 38.5$; however, the backscatter for $\tau_0^* = 7.74$

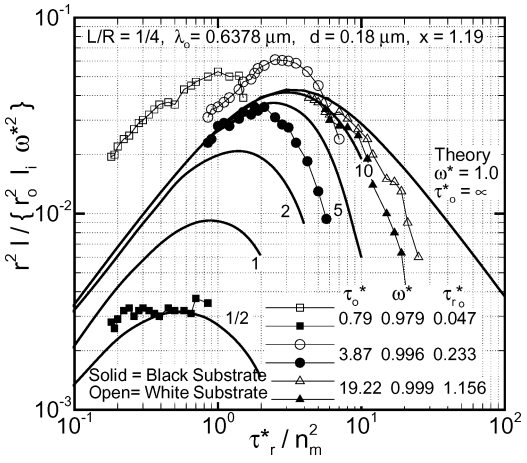

Fig. 16 Nondimensional backscattered intensity from 0.18-μm-diam polystyrene latex particles in distilled water vs contracted effective optical radius τ_r^*/n_m^2 ($L/R = 1/4$; ■, ▲, ●, black substrate; □, △, ○ white substrate).[19]

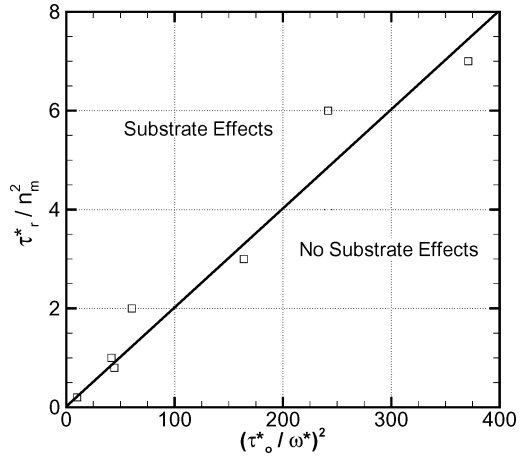

Fig. 17 Substrate effect boundary. Substrate effects are important for points above the curve.[19]

and 1.57 is highly dependent on the substrate characteristics. The white substrate yields considerably more back scattering at small τ_r^* than the black substrate.

Figure 16 illustrates the backscattered radiation data for $\tau_0^* = 0.79$, 3.87, and 19.22 ($L/R = 1/4$). Substrate effects are very important. Substrate characteristics even affect the back scattering for $\tau_0^* = 19.22$ (a rather large optical depth).

The preceding data for substrates effects can be summarized by plotting the value of τ_r^*, where substrate effects become noticeable as a function of $(\tau_0^*/\omega^*)^2$, as shown in Fig. 17.

The onset of substrate effects can be correlated by the relation

$$\tau_r^* \geq \left(n_m^2/50\right)\left(\tau_0^*/\omega^*\right)^2 \tag{14}$$

Substrate effects depend on both τ_0^* and τ_r^* as well as ω^* and n_m. They are important for all combinations of τ_0^*, τ_r^*, ω^*, and n_m that lie above the line shown in Fig. 17.

Transmission

This section presents comparisons of experimental and theoretical two-dimensional results for laser-beam transmission through a multiple-scattering medium from the work of Nelson and Satish.[20] An azimuthally symmetric He–Ne laser beam with a Gaussian radial distribution was incident normal to a scattering media [see Eq. (1)], consisting of double distilled water and uniform-sized spherical latex particles 0.481 μm in diameter. The transmitted radiation was measured as a function of effective optical radius from the beam τ_r^* and effective optical thickness of the scattering medium τ_0^*. The physical situation for transmission measurements is shown schematically in Fig. 2.

The theoretical solution for the transmitted intensity can be written as the sum of the directly transmitted intensity and the diffuse intensity

$$I_T\left(\tau_r^*, \tau_0^*\right) = \frac{I_i \exp\left[-\left(\tau_r^*/\tau_{r_0}^*\right)^2 - \tau_0^*\right]}{\Delta\Omega} + I_d\left(\tau_r^*, \tau_0^*\right) \tag{15}$$

where τ_0^* is the effective optical thickness of the scattering medium and $\Delta\Omega$ is the incremental solid angle centered on the normal direction. Crosbie[21] has shown that $I_d(\tau_r^*, \tau_0^*)$ for $\tau_r^* \gg \tau_{r_0}^*$ (far from the center of the incident laser beam) can be written as

$$I_d\left(\tau_r^*, \tau_0^*\right) = \left(\frac{\omega^* \tau_{r_0}^*}{4\tau_r^*}\right)^2 \tau_0^* \tau_r^* I_i \exp\left(-\tau_0^*\right) \tag{16}$$

in the double-scattering τ_r^* regime. Equation (16) can be written in nondimensional form as

$$r^2 I_d \Big/ \left(r_0^2 I_i\right) = \omega^{*2} \tau_0^* \tau_r^* \exp\left(-\tau_0^*\right) \Big/ 16 \tag{17}$$

This nondimensional form of the diffuse, double-scattered, transmitted intensity is independent of $\tau_{r_0}^*$ and linear in τ_r^*. One must be careful in applying Eq. (17) because, in multiple-scattering situations at large τ_r^*, the higher-order scattering terms become important, not only because of transmission but also because of reflection from the tank walls.

Figure 18 presents measurements of $r^2 I/(r_0^2 I_i)$ vs τ_r^* for τ_0^* values from 2 to 10.3 for $L/R = 1/3$. The corresponding exact theoretical solutions and double-scattering approximate solutions for isotropic scattering and $\tau_{r_0}^* = 0.01$ are also shown. Comparison to experimental data at different $\tau_{r_0}^*$ values is acceptable because Eq. (17) shows that $r^2 I/(r_0^2 I_i)$ should be independent of $\tau_{r_0}^*$ in this τ_r^* range.

Effective optical values were used to correlate the theory and experiment. The slope of the data at $\tau_{r_0}^* = 2$ is slightly greater than that of the theory. This is because of differences in isotropic phase function used in the theory and the actual phase function of the 0.481-μm particles. The slopes of the theoretical solutions and experimental data agree progressively better as τ_0^* increases because the large number of scattering events tend to reduce the importance of single and double scattering and hence the details of the scattering phase function. The double-scattering approximation is quite good at $\tau_0^* = 2$. However, agreement becomes progressively worse as τ_0^* increases because of the higher-order scattering events.

Figure 18 shows that the experimental and theoretical results agree well at $\tau_0^* = 10$. At $\tau_0^* = 2$ and 5, the experimental data values

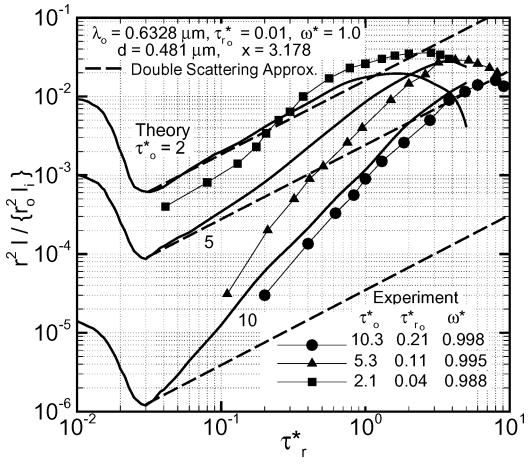

Fig. 18 Experimental and theoretical transmitted intensity for 0.481-μm-diam latex particles in distilled water vs τ_r^* at $\tau_0^* = 2$, 5, and 10 and $L/R = 1/3$: ●, ▲, ■, experimental data; ——, theory; and – – –, double-scattering approximation.[20]

are lower than the theoretical solution at small values of τ_r^*, and they are higher than the theoretical values at large τ_r^*. This is attributed to 1) experimental results being for particles that have a strong forward-scattering lobe, while the theory uses a simple isotropic scattering phase function model; and 2) difficulties in obtaining good data close to the beam center.

The agreement between theory and experiment improves as the particle concentration increases because more scattering events occur. At small particle concentrations, single and double scattering are important; consequently, the angular details of the phase function are important. At higher scattering particle concentrations, more scattering events occur, and they tend to smooth the angular variation of the phase function and make the scattered radiation appear more isotropic. Also, at large τ_0^* and τ_r^* the intensity varies slowly with radius; whereas at small τ_0^* and τ_r^* the intensity has large radial gradients. The detector sees a surface area and averages the intensity over this area. The strong radial gradients cause experimental error at small values of τ_r^*.

Radial Scattering

Scattering of radiation in the radial direction from a laser beam occurs in many practical situations such as underwater visibility, medicine, and defense technology.

Figure 2 is a schematic of the physical situation that was investigated by Nelson and Satish.[22] The laser beam is incident on a scattering medium with finite depth in which it undergoes multiple scattering.

The theoretical expression for the intensity scattered from the laser beam in the radial direction as it propagates through a scattering medium has been developed by Farrell[23] and Crosbie and Farrell.[24] For isotropic, single scattering of a laser beam, the radially scattered intensity is[22]

$$I_R/I_i = \left(\omega/4\sqrt{\pi}\right)\tau_{r_0}\exp\left[-\tau_z - \tau_R + \left(\tau_{r_0}/2\right)^2\right] \qquad (18)$$

when $\tau_{r_0} \ll \tau_R$. For optically thin, single scattering, Eq. (18) can be multiplied by the value of the normalized phase function at 90 deg P_{90} to account for anisotropic scattering. Equation (18) relates the radially scattered intensity inside the scattering medium to the incident intensity. To measure this intensity, the detector was placed outside the glass tank containing the scattering medium. Thus, the radiation had to pass through the glass wall of the tank before it was detected. The refraction at the interface had to be accounted for. An energy balance across the interface yields

$$I = I_R/n_m^2 \qquad (19)$$

where $n_m = 1.33$ at $\lambda_0 = 0.6328\ \mu$m. Therefore, the nondimensional intensity outside the glass wall is

$$\frac{I}{I_i} = \frac{I_R}{n_m^2 I_i} = \frac{\sigma}{4\sqrt{\pi}}\frac{r_0}{n_m^2}\exp\left[-\tau_z - \tau_R + \left(\frac{\tau_{r_0}}{2}\right)^2\right]P_{90} \qquad (20)$$

where the wall thickness of the glass has been ignored and where τ_R and τ_z contain the radial and depth variation. Note that I/I_i is directly proportional to σ and that it decreases linearly with τ_R and τ_z (R and z) for optically thin cases whereas for larger optical depths it decreases exponentially with τ_R and τ_z.

In the limit as optical thickness goes to zero, all of the exponentials go to 1, and I/I_i becomes

$$\frac{I}{I_i} = \frac{\sigma r_0}{4\sqrt{\pi}n_m^2}P_{90} \qquad (21)$$

Thus, in the optically thin limit, for a given set of experimental parameters σ, r_0, n_m, and P_{90} the theoretical radial-scattered intensity does not vary with z or r in the scattering medium.

The experimental situation is shown schematically in Fig. 2. The details of the detection system are given in Nelson and Satish.[22] The normalized scattering phase functions of the 0.091- and 0.481-μm-diam particles immersed in water at $\lambda_0 = 0.6328\ \mu$m were generated using Mie theory and are shown in Fig. 5. The 0.481-μm phase function shows a strong forward-scattering peak, whereas the 0.091-μm particle phase function corresponds closely to a Rayleigh-scattering distribution. Table 3 gives the values of the experimental parameters.

Table 3 Values of experimental parameters

τ_0	τ_{r_0}	ω	σ, 1/cm
	$d = 0.091\ \mu m$		
0.053	0.00055	0.097	0.00054
0.065	0.00069	0.270	0.00185
0.075	0.00079	0.367	0.00290
0.086	0.00090	0.445	0.00401
0.107	0.00113	0.557	0.00628
0.164	0.00173	0.711	0.0123
0.218	0.00230	0.782	0.0180
	$d = 0.481\ \mu m$		
0.220	0.00231	0.784	0.0181
0.258	0.00272	0.816	0.0222
0.322	0.00339	0.852	0.0289
0.386	0.00406	0.877	0.0356
0.482	0.00507	0.901	0.0457
2.426	0.0255	0.980	0.250

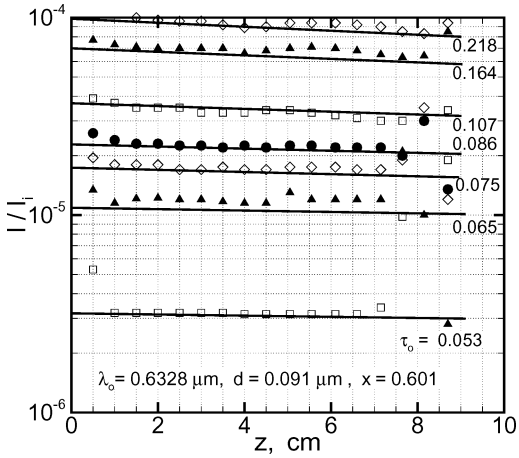

Fig. 19 Experimental (◇, □, ●, ▲) and theoretical (——) side-scattered intensity as a function of depth for 0.091-μm-diam latex particles for a range of optical depths: $L/R = 2$, $P_{90} = 0.755$, $\sigma = 845$ 1/cm, and $\tau_0 = \beta L$ (Ref. 22).

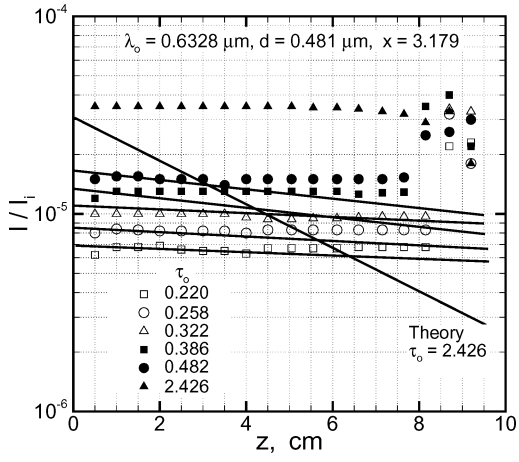

Fig. 20 Experimental (□, △, ○, ■, ▲, ●) and theoretical (——) side-scattered intensity as a function of depth for 0.481-μm-diam latex particles for optical depths up to 2.43: $L/R = 2$, $P_{90} = 0.055$, $\sigma = 22{,}983$ 1/cm, and $\tau_0 = \beta L$ (Ref. 22).

Figures 19 and 20 show comparisons of the experimental and theoretical values of I/I_i as a function of depth below the upper surface of the scattering medium. The theoretical curves were obtained using Eq. (20). Figure 19 shows the optically thin results

for 0.091-μm-diam particles. The value of P_{90} for these particles is 0.755, which implies that there is a large amount of radially scattered intensity. The experimental intensity does not vary with z at small values of τ_0. As τ_0 increases, I/I_i begins to decrease faster with z in agreement with the theoretical predictions. The agreement between the experimental and theoretical values of I/I_i is good over the entire range of τ_0 from 0.053 to 0.22, except near the tank bottom ($z \geq \approx 9$ cm). Reflection of the directly transmitted laser beam from the bottom causes the increase in I/I_i at small τ_0. Figure 19 shows optically thin data.

Figure 20 shows a comparison between experimental and theoretical results for τ_0 from 0.22 to 2.43 when 0.481-μm-diam particles are used as the scattering centers. The value of P_{90} for the 0.481-μm particles is smaller than P_{90} for the 0.091-μm particles, so that the 0.481-μm particles produce less radially scattered intensity for equal values of $\omega\tau_{r_0}$ or σr_0.

As τ_0 increases, the difference between experiment and theory increases, caused by the breakdown of the single-scattering assumption as illustrated by the results shown in Fig. 20 for $\tau_0 \geq 0.4$. At $\tau_0 = 2.426$, the experimental value of I/I_i does not drop very much as z increases; however, the theoretical solution for I/I_i decreases considerably. This difference is caused by multiple scattering, which is not considered in the theory. Inspection of Fig. 20 shows that multiple-scattering effects begin to show up at values of τ_0 as small as 0.25. The agreement between the theory and experiment is poor near the top and bottom of the scattering medium ($z = 0$ or 10) because of the coupling of radiation reflection off the top or bottom surface and the size of the detector solid angle. The detector could not discriminate between reflection and scattering.

The theoretical solution implies that side-scattered intensity is directly proportional to $\omega\tau_{r_0}$ or σr_0 when τ_z and τ_R are small. The data presented in Figs. 19 and 20 confirm this result.

This analysis does not use effective optical coordinates. The effective optical coordinates account for the phase function model when anisotropic scattering is important. The data have been adjusted slightly by multiplying the experimental value of I/I_i by a constant (very close to unity) to force the data to agree with the theory for the smallest τ_0 case and then using the same constant for all of the data shown of the particular figure. This approach essentially compensated for possible errors in the magnitude of the parameters in experimental setup.

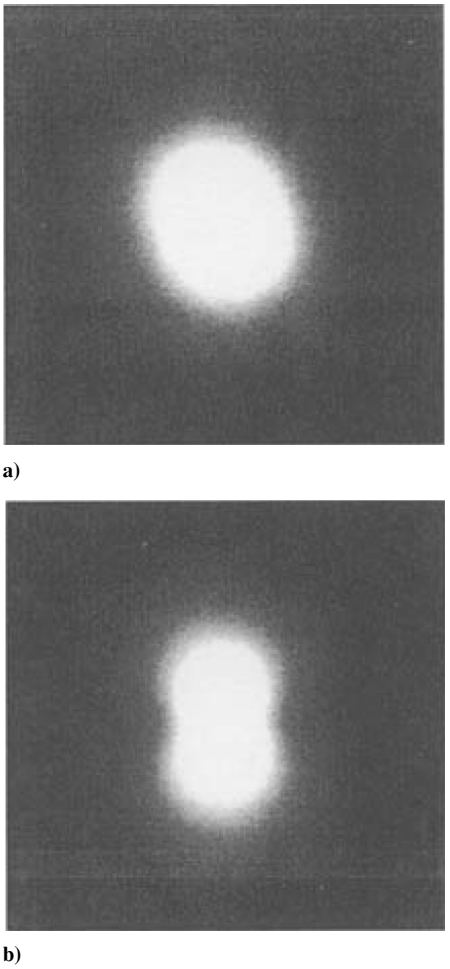

a)

b)

Fig. 21 Backscattered intensity from a medium exposed to a polarized laser beam: a) circularly polarized and b) horizontally linearly polarized. In the photos $d = 0.065$ μm, $\tau_0 \approx 2$, $\tau_{r_0} \approx 0.01$, and laser power = 20 mW (Ref. 26).

Polarization

Effects of multiple scattering on the polarization of laser radiation can be important. Polarization can make an apparently two-dimensional problem become three-dimensional. An example is a Gaussian distributed laser beam perpendicularly incident on the upper surface of a homogeneous, multiple-scattering medium. The laser spatial distribution is cylindrically symmetric. However, the backscattered intensity can actually be three-dimensional, that is, the backscattered intensity is not cylindrically symmetric. Figure 21 shows the intensity backscattered from a tank of distilled water with suspended latex scatterers exposed to a circularly polarized (top) and a horizontally linearly polarized (bottom) helium-neon laser beam. The backscattered radiant intensity exhibits an angular variation for both types of laser polarization. Most radiative-transfer researchers neglect polarization because solution of the vector radiation-transfer equation becomes very complicated. Three-dimensional vector radiative transfer in a semi-infinite, multiscattering exposed to a polarized, Gaussian laser beam directed perpendicularly to the surface has been studied in a series of papers.[25–31]

Ambirajan and Look[32,33] presented a backward Monte Carlo analysis to look at multiple scattering from polarized laser beams. They concluded that the diffuse light field remained partially polarized, even at large optical radii from the incident laser. The degree of polarization was dependent on the optical thickness of the medium and the size parameter of the scattering particles.

Ambirajan and Look[34] experimentally studied the forward-scattered diffuse radiation produced by a circularly polarized laser beam impinging on a finite, plane-parallel scattering medium and compared the results to their Monte Carlo solutions. Mueller and Crosbie[28] numerically investigated radiative transfer in a three-dimensional, semi-infinite, Rayleigh-scattering medium exposed to a polarized, Gaussian laser beam directed normal to the scattering medium surface. The medium was assumed be pure scattering ($\omega = 1$). Rayleigh scattering is valid for spherical particles that are very small compared to the radiation wavelength $x \approx 0$. They investigated the assumption of replacing the Rayleigh-scattering phase matrix with the Rayleigh-scattering phase function $[P(\Theta) = \frac{3}{4}(1 + \cos^2 \Theta)]$. They showed that this approximation can result in errors as large as 20%. Much research remains to be done on the effects of polarization in multiple-scattering media.

Summary

This paper reviews the theoretical and experimental research on anisotropic, multiple-scattering, multiple-dimensional, radiation transfer done at the University of Missouri–Rolla over the past 25 years. The research objective was to develop an anisotropic, multiple-scattering, multiple-dimensional, radiation-transfer theory and verify it experimentally. The scattering medium was two-dimensional and cylindrical because the laser beam was incident normal to the top of the scattering media. The radiative transfer was multidimensional, in that the radiation transport depended on both z and r. Backscattered radiation and transmission were predicted and measured as a function of the radial distance from the incident laser beam. Side scattering was measured and predicted as a function of depth of the scattering medium. The experiments were done using well-characterized latex spheres in distilled water to create the scattering medium. The agreement between the theory and experiment was usually quite good.

Backscattering

This study indicates the following for the radial distribution of the backscattered radiation in the normal direction:

1) As particle size increases, backscattered intensity curve for $r^2 I/(r_0^2 I_i)$ shifts to larger values of τ_r for $x \leq 6.67$.

2) The distribution curves for $r^2 I/(r_0^2 I_i)$ are dependent on g and collapse to a single curve by using $(1-\omega g)$ as a correlation parameter. This reduces the anisotropic scattering situation to an effective isotropic-scattering situation.

3) The maximum value of $r^2 I/(r_0^2 I_i)$ is insensitive to scattering particle size and occurs at $\tau_0^* = 3.345$.

4) The effect of n_m is important and can be accounted for by a $1/n_m^2$ adjustment in τ_r^*.

5) The black substrate results for $r^2 I/(r_0^2 I_i \omega^{*2})$ agree reasonably well with theory.

6) The effects of changing the substrate from black to white are most apparent for small τ_0^* near the laser beam (small τ_r^*); however, substrate effects still occur at large τ_r^* (= 10–15) for τ_0^* values greater than 20. All of this occurs at small L/R.

7) Substrate effects are evident for $\tau_r^* \geq (n_m \tau_0^*/\omega^*)^2/50$.

Transmission

This study indicates the following for the radial distribution of the transmitted radiation in the normal direction:

1) Experimental transmission results compare well with the theoretical scattering results when they are correlated using the effective optical parameters.

2) Anisotropic, multiple scattering is important; however, the effects of the angular details of the scattering phase function tend to be washed out for large τ_0^*.

3) It is very hard to get good direct transmission data (near the beam center) because of the large radial gradients in the radiation.

Radial Scattering

This study indicates the following for the z distribution of the radial-scattered radiation:

1) Experimental radial-scattering values for I/I_i for optically thin media compare well with the single-scattering theoretical solution.

2) Multiple scattering becomes important for $\tau_0 \geq 0.4$.

3) The good agreement between experiment and theory in the optically thin regime shows the validity of the single-scattering theoretical development.

Polarization

This study indicates that polarization is important, and the following were found:

1) A polarized laser beam can cause a two-dimensional geometry to become a three-dimensional situation.

2) Polarization requires the solution of the vector radiation transport equation and makes the analysis very complicated.

3) The backscattered intensity is replaced by a backscattered matrix.

4) A circularly polarized laser beam can be used to reduce three-dimensional effects.

5) Experiments involving polarization are very hard to carry out.

In conclusion one must emphasize that the major portion of this research program studied the scalar radiation-transfer problem in a multidimensional, anisotropic, multiple-scattering medium exposed to a narrow beam of radiation. The exiting radiation was scattered at least twice to leave normal to the surface, and it was a function of both r and z. Multidimensional polarization studies involving anisotropic multiple scattering were done experimentally and theoretically. Polarization effects are very complicated and require the solution of the vector radiation transport equation.

Possible future directions for this research include the following: 1) more realistic boundary conditions, for instance, scattering media refractive index, substrate effects, nonnormal incident radiation, and nonnormal exiting radiation; 2) scattering particles, for instance, larger particles ($x \gg 1$), nonspherical, or hollow particles, voids, and fibers; 3) ordered (matrix) distribution of scattering particles and dependent scattering; 4) nonsteady, for instance, pulsed laser, fluorescent particles; 5) effects of emission and temperature; 6) nonequilibrium effects, for instance, large molecules and chemistry; 7) much more emphasis on polarization effects; and 8) extensions to other scattering geometries, for instance, layered regions, finite rectangular regions, three-dimensional cylindrical regions, and spherical regions. (Looking at three-dimensional situations will become more important in the future.)

Acknowledgment

I thank A. L. Crosbie and D. C. Look for their helpful suggestions in the preparation of this review paper.

References

[1]Drolen, B. L., and Tien, C. L., "Independent and Dependent Scattering in Packed-Sphere Systems," *Journal of Thermophysics and Heat Transfer*, Vol. 1, No. 1, 1987, pp. 63–68.

[2]Look, D. C., Nelson, H. F., Crosbie, A. L., and Dougherty, R. L., "Two-Dimensional Multiple Scattering: Comparison of Theory with Experiment," *Journal of Heat Transfer*, Vol. 100, No. 3, 1978, pp. 480–485.

[3]Look, D. C., Nelson, H. F., and Crosbie, A. L., "Anisotropic Two-Dimensional Scattering: Comparison of Experiment with Theory," *Journal of Heat Transfer*, Vol. 103, No. 1, 1981, pp. 127–134.

[4]Crosbie, A. L., and Davidson, G. W., "Dirac-Delta Function Approximations to the Scattering Phase Function," *Journal of Quantitative Spectroscopy and Radiative Transfer*, Vol. 33, No. 4, 1985, pp. 391–409.

[5]Van de Hulst, H. C., *Multiple Light Scattering*, Vol. 2, Academic Press, New York, 1980, Chaps. 10, 14.

[6]Crosbie, A. L., and Dougherty, R. L., "Two-Dimensional Isotropic Scattering in a Semi-Infinite Cylindrical Medium," *Journal of Quantitative Spectroscopy and Radiative Transfer*, Vol. 20, No. 2, 1978, pp. 151–173.

[7]Crosbie, A. L., and Dougherty, R. L., "Two-Dimensional Linear Anisotropic Scattering in a Semi-Infinite Cylindrical Medium Exposed to a Laser Beam," *Journal of Quantitative Spectroscopy and Radiative Transfer*, Vol. 28, No. 2, 1982, pp. 233–264.

[8]Crosbie, A. L., and Dougherty, R. L., "Two-Dimensional Rayleigh Scattering in a Semi-Infinite Cylindrical Medium," *Journal of Quantitative Spectroscopy and Radiative Transfer*, Vol. 30, No. 3, 1983, pp. 255–280.

[9]Nelson, H. F., "Radiative Scattering Cross Sections: Comparison of Experiment and Theory," *Applied Optics*, Vol. 20, No. 3, 1981, pp. 500–504.

[10]Crosbie, A. L., and Lee, L. C., "Two-Dimensional Anisotropic Scattering in a Semi-Infinite Cylindrical Medium Exposed to a Laser Beam," *Journal of Quantitative Spectroscopy and Radiative Transfer*, Vol. 49, No. 2, 1993, pp. 185–211.

[11]Nelson, H. F., Look, D. C., and Crosbie, A. L., "Two-Dimensional Radiative Back Scattering from Optically Thick Media," *Journal of Heat Transfer*, Vol. 108, No. 3, 1986, pp. 619–625.

[12]Crosbie, A. L., and Lee, L. C., "Single and Double Scattering Approximations for a Two-Dimensional Cylindrical Medium with Anisotropic Scattering," *Journal of Quantitative Spectroscopy and Radiative Transfer*, Vol. 48, No. 4, 1992, pp. 441–466.

[13]Crosbie, A. L., and Dougherty, R. L., "Influence of Refractive Index on the Two-Dimensional Back-Scattering of a Laser Beam: Asymptotic Solutions," *Journal of Quantitative Spectroscopy and Radiative Transfer*, Vol. 40, No. 2, 1988, pp. 123–128.

[14]Crosbie, A. L., and Shieh, S. M., "Three-Dimensional Radiative transfer for Anisotropic Scattering Medium with Refractive Index Greater Than Unity," *Journal of Quantitative Spectroscopy and Radiative Transfer*, Vol. 44, No. 2, 1990, pp. 299–312.

[15]Crosbie, A. L., and Shieh, S. M., "Expansions for Two-Dimensional Back-Scattering from a Semi-Infinite Medium with Refractive Index Greater Than Unity," *Journal of Quantitative Spectroscopy and Radiative Transfer*, Vol. 45, No. 4, 1991, pp. 205–210.

[16]Crosbie, A. L., and Shieh, S. M., "Two-Dimensional Isotropic Scattering in a Semi-Infinite Cylindrical Medium with Refractive Index Greater Than Unity," *Journal of Quantitative Spectroscopy and Radiative Transfer*, Vol. 49, No. 5, 1993, pp. 535–557.

[17]Look, D. C., and Sundvold, P. D., "Anisotropic 2-D Scattering 3: The Effects of Incident Laser Wavelength," *Applied Optics*, Vol. 23, No. 1, 1984, pp. 9–11.

[18]Look, D. C., and Sundvold, P. D., "Anisotropic Two-Dimensional Scattering Part II: Finite Depth and Refractive Index Effects," *AIAA Journal*, Vol. 22, No. 4, 1984, pp. 571, 572.

[19]Nelson, H. F., and Look, D. C., "Substrate Effects on Two-Dimensional Laser Beam Backscattering," *Journal of Thermophysics and Heat Transfer*, Vol. 1, No. 3, 1988, pp. 203–208.

[20]Nelson, H. F., and Satish, B. V., "Transmission of a Laser Beam Through Anisotropic Scattering Media," *Journal of Thermophysics and Heat Transfer*, Vol. 1, No. 3, 1987, pp. 233–239.
[21]Crosbie, A. L., "Single and Double Scattering Approximations for a Two-Dimensional Cylindrical Medium," *Journal of Quantitative Spectroscopy and Radiative Transfer*, Vol. 21, No. 2, 1979, pp. 107–114.
[22]Nelson, H. F., and Satish, B. V., "Radial Scattering of a Laser Beam in Anisotropic Scattering Media," *Journal of Thermophysics and Heat Transfer*, Vol. 2, No. 2, 1988, pp. 104–109.
[23]Farrell, J. B., "Multidimensional Radiative Transfer in a Cylindrical Scattering Medium," M.S. Thesis, Dept. of Mechanical Engineering, Univ. of Missouri–Rolla, Dec. 1981.
[24]Crosbie, A. L., and Farrell, J. B., "Exact Formulation of Multiple Scattering in a Three-Dimensional Cylindrical Geometry," *Journal of Quantitative Spectroscopy and Radiative Transfer*, Vol. 31, No. 5, 1984, pp. 397–416.
[25]Mueller, D. W., and Crosbie, A. L., "Three-Dimensional Radiative Transfer with Polarization in a Multiple Scattering Medium Exposed to Spatially Varying Radiation," *Journal of Quantitative Spectroscopy and Radiative Transfer*, Vol. 57, No. 1, 1977, pp. 81–105.
[26]Mueller, D. W., and Crosbie, A. L., "Analytical Expressions for the Radiation Emergent from a Scattering Medium Exposed to a Polarized Laser Beam," *Journal of Quantitative Spectroscopy and Radiative Transfer*, Vol. 67, No. 6, 2000, pp. 395–428.
[27]Mueller, D. W., and Crosbie, A. L., "Three-Dimensional Vector Radiative Transfer in a Semi-Infinite, Rayleigh Scattering Medium Exposed to a Polarized Laser Beam: Generalized Reflection Matrix," *Journal of Quantitative Spectroscopy and Radiative Transfer*, Vol. 75, No. 1, 2002, pp. 93–120.
[28]Mueller, D. W., and Crosbie, A. L., "Three-Dimensional Vector Radiative Transfer in a Semi-Infinite, Rayleigh Scattering Medium Exposed to a Polarized Laser Beam: Spatially Varying Reflection Matrix," *Journal of Quantitative Spectroscopy and Radiative Transfer*, Vol. 75, No. 4, 2002, pp. 423–453.
[29]Look, D. C., "Anisotropy of the Lateral Scattering of Linearly Polarized Light," *Optical Engineering*, Vol. 28, No. 2, 1989, pp. 160–164.
[30]Look, D. C., and Chen, Y. R., "Study of Polarization of Laser Radiation Scattered 90 Deg," *Journal of Thermophysics and Heat Transfer*, Vol. 7, No. 4, 1993, pp. 631–636.
[31]Look, D. C., and Chen, Y. R., "Examination of Scattering at 90° from a Cylindrical Volume Illuminated by Polarized Light," *Applied Optics*, Vol. 34, No. 1, 1995, pp. 144–150.
[32]Ambirajan, A., and Look, D. C., "A Backward Monte Carlo Estimator for the Multiple Scattering Scattering of a Narrow Light Beam," *Journal of Quantitative Spectroscopy and Radiative Transfer*, Vol. 56, No. 3, 1996, pp. 317–336.
[33]Ambirajan, A., and Look, D. C., "A Backward Monte Carlo Study of the Multiple Scattering Scattering of a Polarized Laser Beam," *Journal of Quantitative Spectroscopy and Radiative Transfer*, Vol. 58, No. 2, 1997, pp. 171–192.
[34]Ambirajan, A., and Look, D. C., "Experiential Investigation of the Multiple Scattering of a Polarized Laser Beam," *Journal of Thermophysics and Heat Transfer*, Vol. 12, No. 2, 1998, pp. 153–163.